



Cite this: *Phys. Chem. Chem. Phys.*, 2025, 27, 1534

# Suboxides and subselenides: intermediate reaction products to form Ga<sub>2</sub>O<sub>3</sub>, Ga<sub>2</sub>Se<sub>3</sub>, In<sub>2</sub>O<sub>3</sub>, In<sub>2</sub>Se<sub>3</sub>, SnO<sub>2</sub>, and SnSe<sub>2</sub> during molecular-beam epitaxy

Patrick Vogt, \*<sup>a</sup> Shun-Li Shang <sup>b</sup> and Zi-Kui Liu <sup>b</sup>

The molecular-beam epitaxial (MBE) growth of III-O and IV-O materials (e.g., Ga<sub>2</sub>O<sub>3</sub>, In<sub>2</sub>O<sub>3</sub>, and SnO<sub>2</sub>) is known to be reaction-limited by complex 2-step kinetics and the desorption of volatile suboxides (e.g., Ga<sub>2</sub>O, In<sub>2</sub>O, SnO). We find that the different surface reactivities of suboxides and respective elements (e.g., Ga, In, Sn) with active oxygen define the film-growth-windows (FGWs) and suboxide-formation-windows (SFWs) of III-O and IV-O materials, respectively. To generalize, we provide elementary reaction pathways and respective Gibbs energies to form binary III-O, III-Se, IV-O, and IV-Se ground-states as well as their subcompounds during their MBE growth. We apply the 2-step kinetics model established for oxides to identify the subselenide-limited growth of Ga<sub>2</sub>Se<sub>3</sub> as the specific example for III-Se materials. Our kinetic and thermodynamic conclusions suggest subcompound-limited growth may be an inherent property for the growth of III-VI and IV-VI thin films by MBE and related epitaxial growth techniques.

Received 25th April 2024,  
 Accepted 18th November 2024

DOI: 10.1039/d4cp01702a

[rsc.li/pccp](http://rsc.li/pccp)

## I. Introduction

In 'classical' molecular-beam epitaxy (MBE) elemental cations react directly with reactive anions to form the intended compound on a heated single-crystalline substrate.<sup>1–4</sup> This is because the MBE growth of III-V and II-VI materials is governed by simple 1-step reaction kinetics.<sup>3,5–10</sup> This basic surface physics and reaction kinetics has been one of the prerequisites to controllably synthesize functional thin films at the highest crystalline level,<sup>11,12</sup> for example, enabling the discovery of novel physics at thin film interfaces.<sup>13</sup>

On the other hand, the MBE growth of III-O and IV-O materials is more complex and determined by complex 2-step reaction kinetics and limited by the formation of volatile suboxides (e.g., Ga<sub>2</sub>O, In<sub>2</sub>O, and SnO).<sup>14–19</sup> These complex surface reactions kinetically prohibit the growth of functional III-O and IV-O thin films in their adsorption-controlled growth regimes.<sup>20,21</sup>

Based on the common valences between III-VI or IV-VI materials, it is conceivable that the growth kinetics of III-Se and IV-Se is similar to that of III-O and IV-O compounds. Previous MBE studies on Ga<sub>2</sub>Se<sub>3</sub> and In<sub>2</sub>Se<sub>3</sub> indicate their growth to be limited by the formation of their subselenides Ga<sub>2</sub>Se and In<sub>2</sub>Se, respectively<sup>22–24</sup>—similar to Ga<sub>2</sub>O<sub>3</sub> and In<sub>2</sub>O<sub>3</sub> being limited by the formation of their suboxides Ga<sub>2</sub>O and In<sub>2</sub>O. However, the underlying reaction

kinetics that form III-Se and IV-Se thin films remains elusive and the lack of microscopically understanding their reaction pathways hinders the full exploration of growth conditions and their impact on the phase formation and material properties of functional selenide-based thin films.<sup>25–29</sup>

In this paper, we start with identifying the surface reactivities ( $\eta_M$ ) of elemental metal (with M = Ga, In, and Sn) as well as the surface reactivities ( $\eta_S$ ) of molecular suboxides (with S = Ga<sub>2</sub>O, In<sub>2</sub>O, and SnO) reacting with oxygen, and find that  $\eta_M \geq \eta_S$ . As a consequence of  $\eta_M \geq \eta_S$ , the film-growth-windows (FGWs) of III-O and IV-O materials fundamentally change upon growth conditions; as we explicitly demonstrate by the example of Ga<sub>2</sub>O<sub>3</sub>. We next model the growth of Ga<sub>2</sub>Se<sub>3</sub> by complex 2-step kinetics and obtain a similar result as established for Ga<sub>2</sub>O<sub>3</sub> growth.<sup>30</sup> To strengthen our model results, we provide elementary reaction pathways and thermodynamic calculations for the Ga<sub>2</sub>O<sub>3</sub>, Ga<sub>2</sub>Se<sub>3</sub>, In<sub>2</sub>O<sub>3</sub>, In<sub>2</sub>Se<sub>3</sub>, SnO<sub>2</sub>, and SnSe<sub>2</sub> growth systems. In all cases, we obtain that suboxides and subselenides are the cationic-like *volatile* species in each material system and we propose that subcompounds (e.g., suboxides and subselenides) are the intermediate and rate-limiting reaction products for III-VI and IV-VI MBE growth, in general.

## II. Suboxide-formation-window (SFW) versus film-growth-window (FGW)

To understand the origin of different surface reactivities between adsorbed metals (e.g., Ga) and formed suboxides (e.g., Ga<sub>2</sub>O)

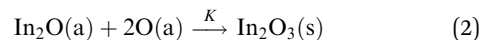
<sup>a</sup> Institute of Solid-State Physics, University of Bremen, Otto-Hahn-Allee 1, Bremen, 28359, Germany. E-mail: p.vogt@kfj.mpg.de

<sup>b</sup> Department of Materials Science and Engineering, Pennsylvania State University, University Park, Pennsylvania 16802, USA



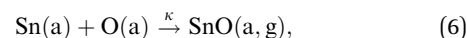
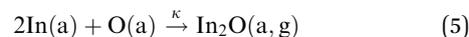
reacting with oxygen, Fig. 1(a)–(g) collect published growth rate ( $\Gamma$ ) data of  $\text{Ga}_2\text{O}_3$ ,<sup>15,31–33</sup>  $\text{In}_2\text{O}_3$ ,<sup>31</sup> and  $\text{SnO}_2$ ,<sup>14</sup> normalized by their respective nominal oxygen flux,  $\phi_{\text{O}}$ . It depicts the fundamental  $\Gamma$  evolutions depending on the metal-to-oxygen flux ratio,  $R = \phi_{\text{M}}/\phi_{\text{O}}$ , at given growth temperature,  $T_{\text{G}}$ , and metal flux,  $\phi_{\text{M}}$ .

We start with the observed  $\Gamma$  plateaus: the solid lines in Fig. 1(a)–(g) reflect the film-growth-windows (FGWs) of  $\text{Ga}_2\text{O}_3$ ,  $\text{In}_2\text{O}_3$ , and  $\text{SnO}_2$ , obtained by experimental data (shown by the open symbols). At elevated  $T_{\text{G}}$ , a  $\Gamma$  plateau emerges and widens with increasing  $T_{\text{G}}$ . We define the value of  $\Gamma$  at the plateau as the value of maximum cation incorporation into the thin film at given  $T_{\text{G}}$ . Based on the 2-step kinetics of these materials,<sup>20,31</sup> this  $\Gamma$  value thus gives the maximum available oxygen reservoir for suboxide-to-oxide formation (S-to-O). This also defines the 2<sup>nd</sup> reaction step to form the oxides  $\text{Ga}_2\text{O}_3$ ,  $\text{In}_2\text{O}_3$ , and  $\text{SnO}_2$ , *via* the reactions:<sup>31</sup>



with reaction rate constant,  $K$ . Adsorbate and solid phases are denoted as a and s, respectively.

To explain the origin of the  $\Gamma$  plateau as well as the onset of the  $\Gamma$  decrease, we now define the suboxide-reaction-window (SRW) for metal-to-suboxide formation (M-to-S). This defines the 1<sup>st</sup> reaction step to form  $\text{Ga}_2\text{O}$ ,  $\text{In}_2\text{O}$ , and  $\text{SnO}$  through forming the suboxides  $\text{Ga}_2\text{O}$ ,  $\text{In}_2\text{O}$ , and  $\text{SnO}$ , respectively, *via* the reactions:<sup>31</sup>



with reaction rate constant,  $\kappa$ . The gaseous phase is denoted as g and refers to the volatility of suboxides during growth. The SRW is indicated by the dotted lines in Fig. 1(b)–(e) and (g) and obtained by extending the  $\Gamma$  evolutions from extending the M-rich growth regime (the *decreasing*  $\Gamma$  with  $\phi_{\text{M}}$ ) as well as the O-rich regime (the *increasing*  $\Gamma$  with  $\phi_{\text{M}}$ ) until both lines intersect—always forming a triangular shape. The suboxides formed during the 1<sup>st</sup> reaction step, eqn (4)–(6), can be further oxidized to the solid compound through a 2<sup>nd</sup> reaction step, eqn (1)–(3), or desorb from the growth surface and limit  $\Gamma$ . As a result, the SRW for M-to-S formation is equal to or wider than the FGW for S-to-O formation, *i.e.*,  $\kappa \geq K$ , depending on  $T_{\text{G}}$ . To illustrate their quantitative differences, the maximum (normalized) formation rates of  $\text{Ga}_2\text{O}$  and  $\text{Ga}_2\text{O}_3$  as well as of  $\text{In}_2\text{O}$  and  $\text{In}_2\text{O}_3$  are plotted as a function of  $T_{\text{G}}$  in Fig. 1(h). A detailed explanation of this effect is given in Fig. 2. The maximum suboxide formation is defined as the peak value of the SRWs, seen by dotted lines in Fig. 1(b)–(d) and (g). In the case of  $\text{SnO}_2$ , we obtain the suboxide formation is about  $1.4\Gamma$  for all  $\phi_{\text{O}}$  at  $T_{\text{G}} = 650$  °C. Overall, the reactivity of  $\text{Sn} > \text{In} > \text{Ga}$  with O is higher than the one of  $\text{SnO} > \text{In}_2\text{O} > \text{Ga}_2\text{O}$  with O, respectively. This feature can also be referred to the different vapor pressures and surface reactivities of the respective elements and suboxides.<sup>16,18,34–38</sup>

Fig. 1(f) and (g) depict the  $\Gamma$  evolutions of  $\text{In}_2\text{O}_3$  and  $\text{SnO}_2$ , respectively, as a function of  $R$ , showing qualitatively the same kinetic behaviour as observed for  $\text{Ga}_2\text{O}_3$ . The quantitative differences in  $\Gamma$  between III-O and IV-O materials arise from the different group III-O and IV-O suboxide stoichiometries as well as their different surface reactivities.<sup>16,37</sup>

Note, for the sake of simplicity, reactions (1)–(6) are selected as specific examples but may be generalized for other III-O and IV-O materials. For example, the knowledge of the 2-step reaction kinetics was used to form  $\text{Al}_2\text{O}_3$ ,<sup>40</sup> rutile  $\text{GeO}_2$ ,<sup>41</sup> or amorphous  $\text{GeO}_2$ <sup>42</sup> *via* the formation of their suboxides  $\text{Al}_2\text{O}$  and  $\text{GeO}$ , respectively. We further note that a ‘direct reaction’ to form the solid-state compound, *e.g.*, *via*  $2\text{Ga} + 3\text{O} \rightarrow \text{Ga}_2\text{O}_3$ , can be kinetically excluded. This assumption is reasonable as the formation of complex compounds can be (usually) described by

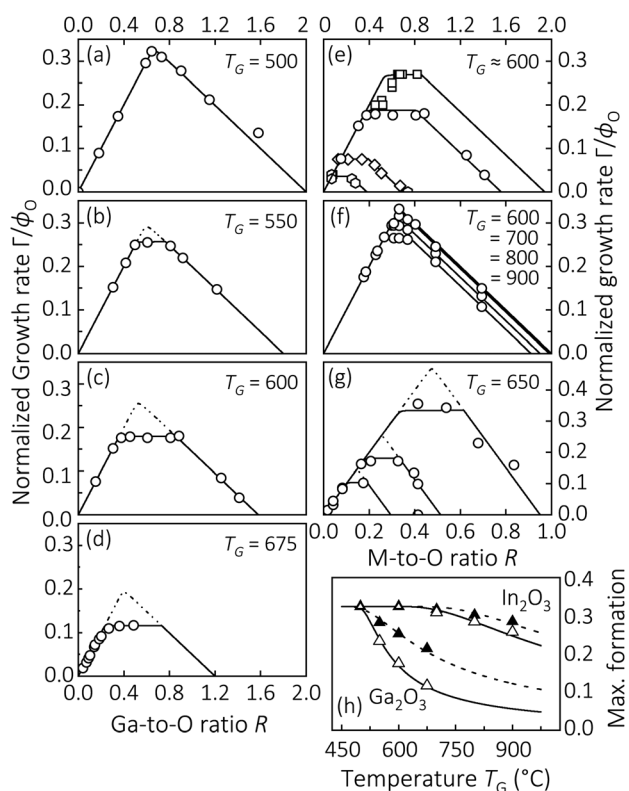


**Fig. 1** (a)–(d)  $\Gamma$  normalized by  $\phi_{\text{O}}$  ( $\Gamma/\phi_{\text{O}}$ ) of  $\beta\text{-Ga}_2\text{O}_3$  ( $\bar{2}01$ ) as a function of the Ga-to-O ratio ( $R = \phi_{\text{Ga}}/\phi_{\text{O}}$ ), measured at different  $T_{\text{G}}$ . Data is taken from ref. 31. (e)  $\Gamma/\phi_{\text{O}}$  as a function of  $R$  of  $\beta\text{-Ga}_2\text{O}_3$  ( $101$ ) [squares],  $\beta\text{-Ga}_2\text{O}_3$  ( $\bar{2}01$ ) [discs, same data as shown in panel (c)],  $\beta\text{-Ga}_2\text{O}_3$  ( $001$ ) [diamonds], and  $\beta\text{-Ga}_2\text{O}_3$  ( $100$ ) [hexagons]. Data is taken from ref. 15 and 31–33. (f)  $\Gamma/\phi_{\text{O}}$  of bixbyite  $\text{In}_2\text{O}_3$  ( $111$ ) as a function of the In-to-O ratio ( $R = \phi_{\text{In}}/\phi_{\text{O}}$ ), measured at different  $T_{\text{G}}$ . Data is taken from ref. 17. (g)  $\Gamma/\phi_{\text{O}}$  of  $\text{SnO}_2$  ( $101$ ) as a function of the Sn-to-O flux ratio ( $R = \phi_{\text{Sn}}/\phi_{\text{O}}$ ), obtained at different  $\phi_{\text{O}}$ . Data is taken from ref. 14. (h) Growth-system-dependent maximum M-to-S formation (solid triangles) [eqn (4)–(6)] and maximum S-to-O formation (*i.e.*, the maximum  $\Gamma$ , open triangles) [eqn (1)–(3)] as a function of  $T_{\text{G}}$ . Symbols represent experimental data, solid and dotted lines are numeric models<sup>18,31</sup> serving as guides to the eye.



a set of elementary reactions rather than by *non*-elementary reactions.<sup>43</sup> In other words, forming the oxide thin film *via* a set of multiple elementary surface reactions *via* a suboxide formation step is kinetically preferred over a single *non*-elemental surface reaction step. As the suboxide itself may also undergo a multi-step reaction pathway, we propose a general reaction scheme to form binary III–VI and IV–VI materials and sketch their possible reaction pathways in Fig. 5 (see below).

### A. Surface-orientation $\Gamma$ dependence of Ga<sub>2</sub>O<sub>3</sub>

Fig. 1(e) shows the comparison of  $\beta$ -Ga<sub>2</sub>O<sub>3</sub> FGWs for different surface orientations of  $\beta$ -Ga<sub>2</sub>O<sub>3</sub>(010),  $\beta$ -Ga<sub>2</sub>O<sub>3</sub>( $\bar{2}$ 01),  $\beta$ -Ga<sub>2</sub>O<sub>3</sub>(001), and  $\beta$ -Ga<sub>2</sub>O<sub>3</sub>(100) as a function of  $R$ , at otherwise similar growth conditions.<sup>15,17,32,33</sup> At given  $T_G \approx 600$  °C,<sup>15,31–33</sup> the orientation dependence of  $\Gamma$  on the ( $hkl$ ) plane,  $\Gamma_{(hkl)}$ , for  $\beta$ -Ga<sub>2</sub>O<sub>3</sub> is quantified as

$$\Gamma_{(010)} \approx 1.5\Gamma_{(\bar{2}01)} \approx 3.7\Gamma_{(001)} \approx 7.7\Gamma_{(100)}. \quad (7)$$

Note this quantification depends on the adsorption and desorption kinetics of Ga<sub>2</sub>O on the respective  $\beta$ -Ga<sub>2</sub>O<sub>3</sub> ( $hkl$ ) growth plane and strongly depends on  $T_G$ .<sup>15,30,44</sup> For example, at  $T_G = 500$  °C the relation  $\Gamma_{(010)} \approx 2.1\Gamma_{(\bar{2}01)}$  was observed,<sup>20</sup> suggesting a different functional dependence of sticking coefficients on the respective Ga<sub>2</sub>O<sub>3</sub> growth surface. We thus qualitatively propose, the orientation-dependent  $\Gamma$  evolution of Ga<sub>2</sub>O<sub>3</sub> can be explained by an interplay of the corresponding orientation-dependent O sticking coefficients ( $\sigma$ ) and suboxide surface reactivities  $\eta_S$ , leading to:

$$\Gamma_{(010)} > \Gamma_{(\bar{2}01)} > \Gamma_{(001)} > \Gamma_{(100)}. \quad (8)$$

A similar orientation-dependent  $\Gamma$  of  $\beta$ -Ga<sub>2</sub>O<sub>3</sub> in binary Ga–O and Ga<sub>2</sub>O–O systems is reported in ref. 18, 33 and 44.

### B. Suboxides limiting the growth domain of III–O compounds

For all compounds, we find that  $SRW \geq FGW$ , thus, the physical origin of changing FGWs and emerging  $\Gamma$  plateaus can now explained.

Fig. 2(a) sketches the  $\Gamma$  evolutions of Ga<sub>2</sub>O<sub>3</sub> ( $\bar{2}$ 01) at  $T_G = 500$  °C (the gray shaded area) and  $T_G = 600$  °C (the purple shaded area), see also Fig. 1(a) and (c). Four regimes are indicated: (i) the O-rich growth regime, *i.e.*, the *increasing*  $\Gamma$  with increasing Ga flux,  $\phi_{Ga}$ . In this regime, enough O adsorbates are available to fully oxidize all adsorbed Ga *via* the consecutive reaction  $Ga \rightarrow Ga_2O \rightarrow Ga_2O_3$  [reactions (4) and (1)]. (ii) The ‘pseudo’ O-rich growth regime identified by the width of the  $\Gamma$  plateau,  $\lambda$ . Here, enough O adsorbates are available to oxidize all adsorbed Ga to its suboxide *via*  $Ga \rightarrow Ga_2O$  [reaction (4)] but not enough O is available to oxidize all formed suboxides to its solid-state compound *via*  $Ga_2O \rightarrow Ga_2O_3$  [reaction (1)]—due to thermally-induced suboxide desorption. In other words, the  $\Gamma$  plateau emerges once the formed Ga<sub>2</sub>O adsorbate density exceeds the O adsorbate density available for reaction  $Ga_2O \rightarrow Ga_2O_3$  [reaction (1)].<sup>21</sup> (iii) The Ga-rich growth regime identified by the *decreasing*  $\Gamma$  with  $\phi_{Ga}$  and its width,  $\omega$ . Here, not enough O is available to oxidize all remaining suboxides to its solid-state compound *via*  $Ga_2O \rightarrow Ga_2O_3$  [reaction (1)]. Now, this is due to an O-deficient-induced suboxide desorption mechanism—in addition to the thermally-induced suboxide desorption identified for regime (ii). (iv) The *no*-growth regime where Ga<sub>2</sub>O<sub>3</sub> growth ceases for  $R \geq R_m$ . Here, not enough O is available to oxidize  $Ga \rightarrow Ga_2O$  [reaction (4)] and reaction (1) becomes kinetically *forbidden* as all available O is consumed in reaction (4).

We next answer the question: Why does  $\Gamma$  start to decrease at  $R^o$  [see Fig. 2(a)] and regime (iii) is entered? Each leaving

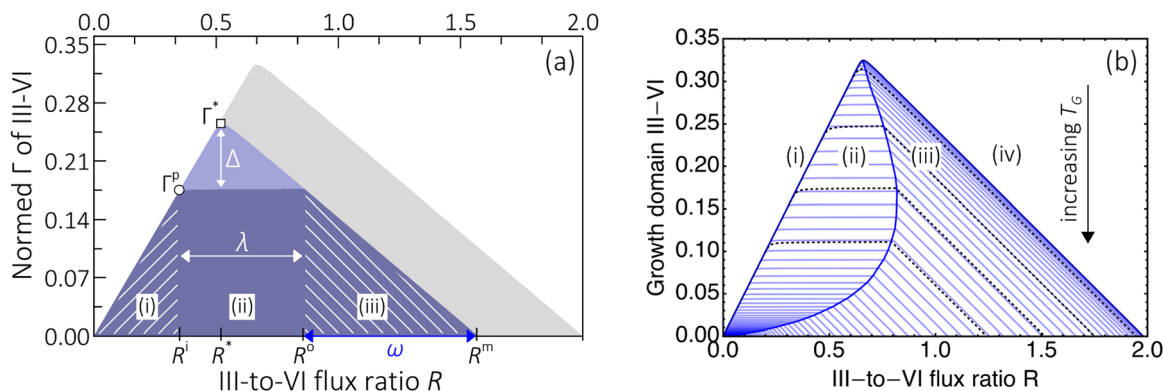


**Fig. 2**  $\Gamma$  evolutions for III–O compounds, explicitly drawn for Ga<sub>2</sub>O<sub>3</sub>. Four distinct growth regimes (i)–(iv) are identified (details provided in the text). (a) The gray and purple areas reflect the modelled film-growth-windows (FGWs) for Ga<sub>2</sub>O<sub>3</sub> based on the data obtained at  $T_G = 500$  °C [Fig. 1(a)] and  $T_G = 600$  °C [Fig. 1(c)], respectively. The difference ( $\Delta$ ) between SFW and FGW for Ga-to-Ga<sub>2</sub>O formation [eqn (4)] and Ga<sub>2</sub>O-to-Ga<sub>2</sub>O<sub>3</sub> formation [eqn (1)] is drawn as the pale purple area at  $T_G = 600$  °C. At  $T_G = 500$  °C this difference is zero, *i.e.*,  $\Delta = 0$ . The length of the  $\Gamma$  plateau is given by  $\lambda$  [regime (ii)] and the width of regime (iii) is defined as  $\omega$ . All parameters shown here are collected in Table 1. (b) FGWs of Ga<sub>2</sub>O<sub>3</sub> as a function of  $R$  modelled for  $400$  °C  $\leq T_G \leq 1200$  °C (the pale blue lines), using a numerical approach based on the models given in ref. 18 and 39. At low  $T_G = 400$  °C, the triangular shape defines the maximum accessible  $\eta_M = \eta_S \Rightarrow SRF = FGW$  (the dark blue line) divided in regimes (i), (iii), and (iv). With increasing  $T_G$ , regime (ii) emerges and the ‘shape’ of the FGW fundamentally changes to a trapezoidal shape due to  $\eta_M > \eta_S \Rightarrow SRF > FGW$  (the dark blue line in the center). The fact that  $SRF \geq FGW$ , changes  $\lambda$ ,  $\Delta$ , and  $\omega$ , depending on  $T_G$ . As a consequence, regime (iii) becomes narrower until it vanishes at high  $T_G$ . The black dashed lines correspond to the solid black model lines in Fig. 1(a)–(d) and serve as a guide to the eye.



Ga<sub>2</sub>O that cannot be oxidized removes 2 × Ga but only 1 × O from the growth front, producing a more O-rich Ga-to-O surface ratio than expected from the nominally supplied  $\phi_{\text{Ga}}$  and  $\phi_{\text{O}}$ . Nevertheless, for  $R > R^0$ ,  $\phi_{\text{Ga}}$  and resulting Ga adsorbate density exceed a critical value, resulting in a Ga-rich growth surface and thus regime (iii) is entered. In this regime, not enough O is available to oxidize all formed Ga<sub>2</sub>O that have remained on the growth surface (*i.e.*, Ga<sub>2</sub>O molecules that have not desorbed), and  $\Gamma$  decreases due to the O-surface-deficiency-induced suboxide desorption. As specific example, all parameters and values for Ga<sub>2</sub>O<sub>3</sub> are indicated in Fig. 2(a) and collected in Table 1, which, in turn, are extracted from the data plotted in Fig. 1(a)–(d). After considering all desorbing species, it is found that the Ga<sub>2</sub>O<sub>3</sub> growth surface becomes stoichiometric once

$$\frac{\phi_{\text{Ga}}}{\phi_{\text{O}}} \geq \frac{2\Gamma^{\text{p}}}{\frac{1}{2}(3R^* - \lambda)} = \frac{n_{\text{Ga}}}{n_{\text{O}}} = \frac{x}{y}, \quad (9)$$

see Fig. 2 and Table 1.

The above findings have fundamental consequences for the  $\Gamma$  evolution of III–VI and IV–VI compounds. For example,  $\lambda$  increases and  $\omega$  decreases with increasing  $T_{\text{G}}$  because of the enhanced thermally-induced suboxide desorption. As a result, the ‘shape’ of the accessible FGW changes upon growth conditions. Based on the data plotted in Fig. 1(a)–(d), Fig. 2(b) now depicts such an  $\Gamma$  evolution as a function of  $R$  and different  $T_{\text{G}}$  (here of Ga<sub>2</sub>O<sub>3</sub>).

At low  $T_{\text{G}}$ , the triangular shape of the modeled  $\Gamma$  defines the maximum possible FGW for these materials. With increasing  $T_{\text{G}}$ , the  $\Gamma$  plateau emerges and the growth domain becomes trapezoidal and narrows until growth eventually ceases. This finding reveals that the growth of Ga<sub>2</sub>O<sub>3</sub> in the Ga-rich regime and elevated  $T_{\text{G}}$  is hardly possible, associated with extremely slow  $\Gamma$ . Nevertheless, these growth conditions are desired to improve the crystallographic and transport properties of Ga<sub>2</sub>O<sub>3</sub> grown by conventional MBE.<sup>28</sup> The same argument holds for In<sub>2</sub>O<sub>3</sub>, for example.

A solution to overcome these intrinsic and detrimental growth limits for group III and group IV oxides is the use of recent advances in their thin film synthesis, such as *suboxide* MBE (*S*-MBE),<sup>20,21,45</sup> metal-exchange catalysis (MEXCAT)<sup>18,37</sup> with metal-oxide-catalyzed epitaxy (MOCATAXY),<sup>17,46</sup> thermal laser epitaxy (TLE),<sup>40</sup> or hybrid MBE (*h*MBE).<sup>47,48</sup>

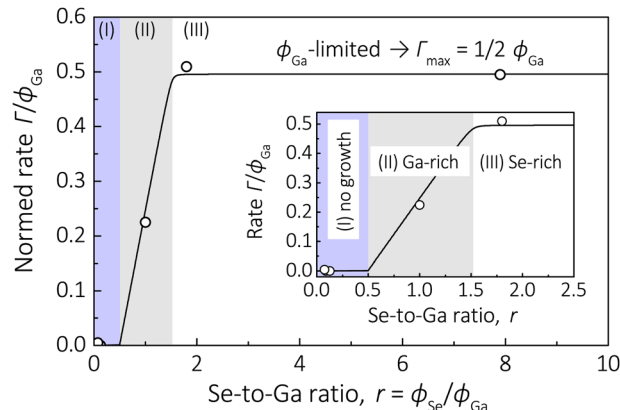


Fig. 3 Normalized  $\Gamma/\phi_{\text{Ga}}$  of  $\alpha$ -Ga<sub>2</sub>Se<sub>3</sub> as a function of the Se-to-Ga flux ratio,  $\phi_{\text{Se}}/\phi_{\text{Ga}} = r$ . Data is taken from ref. 22, Ga and Se densities in  $\alpha$ -Ga<sub>2</sub>Se<sub>3</sub><sup>49</sup> are used to convert  $\phi_{\text{Ga}}$ ,  $\phi_{\text{Se}}$ , and  $\Gamma$  into nm<sup>-2</sup> s<sup>-1</sup>. The solid black line is the application of the 2-step model to the experimental data. The data and model shown in the main graph and the inset are complementary but displayed for the sake of readability. In the Se-rich regime,  $\Gamma$  is maximized and limited by the supplied  $\phi_{\text{Ga}}$ . Note, the horizontal axis in this graph is swapped when compared to the horizontal axes in Fig. 1.

These findings can also be transferred to IV-O materials, *e.g.*, SnO<sub>2</sub>. In contrast to the ‘asymmetric’  $\Gamma$  plateau observed for III-O materials (Fig. 2), the  $\Gamma$  plateau observed for IV-O materials is ‘symmetric’ as plotted for SnO<sub>2</sub> in Fig. 1(g). The occurrence of an asymmetric  $\Gamma$  plateau (III–VI) or symmetric  $\Gamma$  plateau (IV–VI) can be explained by the different stoichiometries of III-O and IV-O suboxides. For example, during the growth of SnO<sub>2</sub> the desorption of SnO removes 1 × Sn and 1 × O, resulting in the observed symmetric  $\Gamma$  plateau. In contrast to SnO<sub>2</sub>, during the growth of Ga<sub>2</sub>O<sub>3</sub> the desorption of Ga<sub>2</sub>O removes 2 × Ga and 1 × O, resulting in the observed asymmetric  $\Gamma$  plateau. Another quantitative consequence of the different suboxide stoichiometries is the differently observed slopes in their M-rich regimes for III-O and IV-O materials with

$$\left(\frac{\partial\Gamma_{\text{III-O}}}{\partial R}\right)_{\text{M-rich}} = -\frac{1}{2} \quad (10)$$

$$\left(\frac{\partial\Gamma_{\text{IV-O}}}{\partial R}\right)_{\text{M-rich}} = -1,$$

respectively. For example, see Fig. 1(a) for III-O and Fig. 1(g) for IV-O materials.

**Table 1** Stoichiometric M-to-O flux ratio,  $R^*$ . Maximum suboxide formation rate,  $\Gamma^*$ , for Ga-to-Ga<sub>2</sub>O oxidation. The growth rate value at the plateau,  $\Gamma^{\text{p}}$ . Maximum flux ratio where Ga<sub>2</sub>O<sub>3</sub> growth is possible,  $R^{\text{m}}$ . The flux ratio at the beginning of the plateau,  $R^{\text{i}}$  (with ‘i’ for in). The flux ratio at the end of the plateau,  $R^{\text{o}}$  (with ‘o’ for out). The maximum Ga adsorbates,  $n_{\text{Ga}}$ , and the maximum O adsorbates,  $n_{\text{O}}$ . The difference  $\Delta$  between the Ga<sub>2</sub>O SRW and the Ga<sub>2</sub>O<sub>3</sub> FGW. The length  $\lambda$  of the plateau and the width  $\omega$  of the Ga-rich regime (ii). Finally, the Ga-to-O adsorbate ratio at the end of the plateau,  $n_{\text{Ga}}/n_{\text{O}} = x/y = \text{constant} \leq \phi_{\text{Ga}}/\phi_{\text{O}}$  [see eqn (9)]. Parameters are indicated in Fig. 2(a) and values are extracted from the data shown in Fig. 1(a)–(d). This example may serve as a blueprint for all discussed III–VI and IV–VI materials

$T_{\text{G}}$ (°C)	$R^* = 2\Gamma^* = 1/3R^{\text{m}}$	$R^{\text{i}} = n_{\text{Ga}} = 2\Gamma^{\text{p}}$	$R^{\text{o}}$	$\lambda = R^{\text{o}} - R^{\text{i}}$	$n_{\text{O}} = 1/2(3R^* - \lambda)$	$\Delta = \Gamma^* - \Gamma^{\text{p}}$	$\omega = 3R^* - R^{\text{o}}$	$n_{\text{Ga}}/n_{\text{O}}$
500	2/3	2/3	2/3	0	1	0	4/3	≈2/3
550	0.58	0.48	0.79	0.31	0.72	0.05	0.97	≈2/3
600	0.52	0.36	0.85	0.49	0.54	0.08	0.71	≈2/3
675	0.48	0.24	0.97	0.73	0.36	0.12	0.42	≈2/3



### III. Subselenide-limited growth of Ga<sub>2</sub>Se<sub>3</sub>

The formation of suboxides has been experimentally reported<sup>14–16</sup> and identified as the growth-limiting step for III–O and IV–O materials and reaction-rate models describing the complex 2-step kinetics for these materials have been developed.<sup>18,31</sup> We anticipate the same kinetics and models can be applied to other III–VI and IV–VI compounds. Therefore, we now apply the 2-step model to the growth of III–Se materials, explicitly, to the growth of Ga<sub>2</sub>Se<sub>3</sub>.

Fig. 3 shows the  $\Gamma$  evolution of Ga<sub>2</sub>Se<sub>3</sub> as a function of the Se-to-Ga ratio,  $r$ . The 2-step model described above for oxides is applied to the data and describes the growth kinetics for Ga<sub>2</sub>Se<sub>3</sub> very accurately—indicating its MBE growth is limited by Ga<sub>2</sub>Se desorption. A similar  $\Gamma$ -behavior is also reported for the growth of In<sub>2</sub>Se<sub>3</sub> by MBE.<sup>23</sup> In ref. 22 and 23, it was speculated that the growth of Ga<sub>2</sub>Se<sub>3</sub> and In<sub>2</sub>Se<sub>3</sub> ceases in the excess of Ga and In fluxes, respectively, due to the re-evaporation of the Ga and Se compounds. However, the physical origin for the observed  $\Gamma$  evolutions for Ga<sub>2</sub>Se<sub>3</sub> and In<sub>2</sub>Se<sub>3</sub> remained elusive.<sup>22,23</sup> The black lines in Fig. 3 show numeric model calculations by a subselenide-mediated 2-step model. Three distinct regimes are identified: (I) no growth regime for  $0 < r = \phi_{\text{Se}}/\phi_{\text{Ga}} \leq 1/2$ , because all reactive Se is consumed for Ga<sub>2</sub>Se formation, *i.e.*,  $r = 1/2$  defines the stoichiometric flux ratio for  $2\text{Ga} + \text{Se} \rightarrow \text{Ga}_2\text{Se}$  formation, *e.g.*, *via* reaction (14). (II) The Ga-rich regime is entered for  $1/2 < r \leq 3/2$ , because not enough reactive Se is available to convert  $\text{Ga}_2\text{Se} \rightarrow \text{Ga}_2\text{Se}_3$ , *e.g.*, *via* reaction (15). The stoichiometric flux ratio for Ga<sub>2</sub>Se<sub>3</sub> formation is thus  $r = 3/2$ . (III) For  $r > 3/2$  the Se-rich flux regime is entered and enough reactive Se is available to selenize  $\text{Ga} \rightarrow \text{Ga}_2\text{Se} \rightarrow \text{Ga}_2\text{Se}_3$ .  $\Gamma$  is now limited by the supplied  $\phi_{\text{Ga}}$ .

Based on the data shown in Fig. 1–3, we can now generalize eqn (10) for III–VI and VI–VI materials for the anion-rich regime (A), plateau regime (P), and cation-rich regime (C) as

$$\left(\frac{\partial\Gamma}{\partial R}\right)_A = y - x, \quad \left(\frac{\partial\Gamma}{\partial R}\right)_P = 0, \quad \left(\frac{\partial\Gamma}{\partial R}\right)_C = 1 - \frac{y}{x}. \quad (11)$$

### IV. Thermodynamic analysis and surface reactions

To support and strengthen our prediction that suboxides and subselenides limit the growth of oxides and selenides, respectively, we now perform thermodynamical calculations. Equilibrium calculations are performed using the SGTE substance database (SSUB5)<sup>50</sup> within the Thermo-Calc software<sup>51</sup> to assess the evaporation behavior of cation-like and anion-like species as a function of temperature of the binary oxides Ga<sub>2</sub>O<sub>3</sub>, In<sub>2</sub>O<sub>3</sub>, and SnO<sub>2</sub> and the complementary, binary selenides Ga<sub>2</sub>Se<sub>3</sub>, In<sub>2</sub>Se<sub>3</sub>, and SnSe<sub>2</sub>. The results are plotted in Fig. 4.

For the investigated compounds Ga<sub>2</sub>O<sub>3</sub>, In<sub>2</sub>O<sub>3</sub>, SnO<sub>2</sub>, In<sub>2</sub>Se<sub>3</sub>, and SnSe<sub>2</sub>, we find that the most volatile, cationic-like species at relevant  $T_{\text{G}}$  are the suboxides and subselenides Ga<sub>2</sub>O, In<sub>2</sub>O,

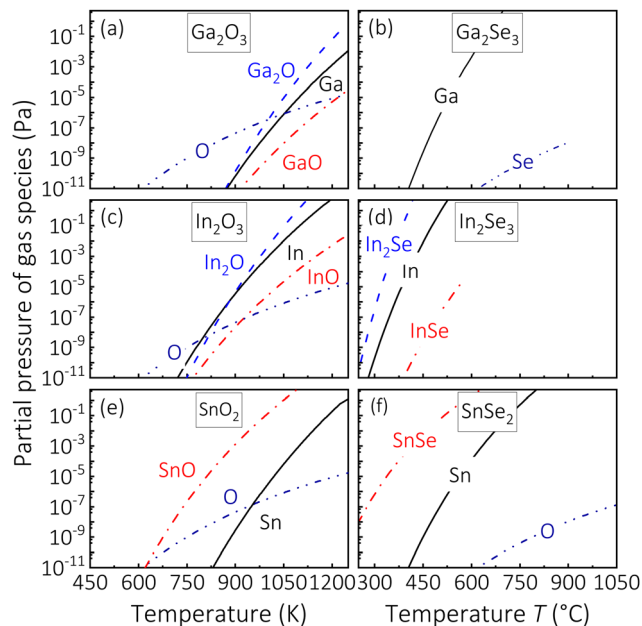


Fig. 4 (a) Calculated partial pressures of the gas species  $C = \text{Ga}, \text{In}, \text{Sn}$ ,  $A = \text{O}, \text{Se}$ ,  $C_{y-x}A_{y-x} = \text{GaO}, \text{InO}, \text{InSe}, \text{SnO}, \text{SnSe}$  [reaction (12)], and  $C_xA_{y-x} = \text{Ga}_2\text{O}, \text{In}_2\text{O}, \text{In}_2\text{Se}$  [reactions (13) and (14)].

SnO, In<sub>2</sub>Se, and SnSe, respectively, and are in accordance with our kinetics findings that their growth is reaction-limited by subcompound formation and their subsequent desorption. Note, for the Ga<sub>2</sub>Se<sub>3</sub> system, the subselenides GaSe and Ga<sub>2</sub>Se are missing in the SSUB5 and other thermodynamic databases, thus, we use the kinetic data shown in Fig. 3 to identify that the growth of Ga<sub>2</sub>Se<sub>3</sub> is reaction-limited by the subselenide Ga<sub>2</sub>Se. This is in agreement with all other investigated growth systems. For example, if Ga was the volatile, cationic species limiting the growth of Ga<sub>2</sub>Se<sub>3</sub>,  $\Gamma$  would reach a plateau in the Ga-rich regime instead, being similar to the growth kinetics observed for binary III–N compounds.<sup>8</sup> The fact that  $\Gamma$  of Ga<sub>2</sub>Se<sub>3</sub> and In<sub>2</sub>Se<sub>3</sub> decrease in the Ga-rich and In-rich regimes, respectively, can thus be explained by the desorption of Ga<sub>2</sub>Se and In<sub>2</sub>Se. We note that the desorption of GaSe and InSe would also explain a decreasing  $\Gamma$  in the cation-rich regimes but with different slopes as given in eqn (11).

In addition, calculated Gibbs energies ( $\Delta G$ ) to form Ga<sub>2</sub>Se<sub>3</sub> further strengthen our hypothesis of a 2-step reaction kinetics underlying the formation of III–Se compounds. To unambiguously identify the growth-rate-limiting steps of Ga<sub>2</sub>Se<sub>3</sub> and In<sub>2</sub>Se<sub>3</sub>, *in situ* line-of-sight mass spectroscopy will reveal which subcompound is formed on the respective growth surface.

To microscopically understand the observed and modeled  $\Gamma$  evolutions (Fig. 1–3) and evaporation of suboxides and subselenides, a general reaction scheme for III–VI and IV–VI compounds is proposed in Fig. 5. It depicts a  $C_xA_y$  layer (*e.g.*, Ga<sub>2</sub>Se<sub>3</sub>), impinging cation flux  $\phi_c$  and anion flux  $\phi_a$ , producing the cation (C), anion (A), and subcompound surface populations  $C_{y-x}A_{y-x}$  (*e.g.*, GaSe),  $C_xA_{y-x}$  (*e.g.*, Ga<sub>2</sub>Se),  $C_xA_{2(y-x)}$  (*e.g.*, Ga<sub>2</sub>Se<sub>2</sub>). Stoichiometric coefficients for III–VI and IV–VI materials are  $x = 2$  and  $y = 3$  as well as  $x = 1$  and  $y = 2$ , respectively. The reaction



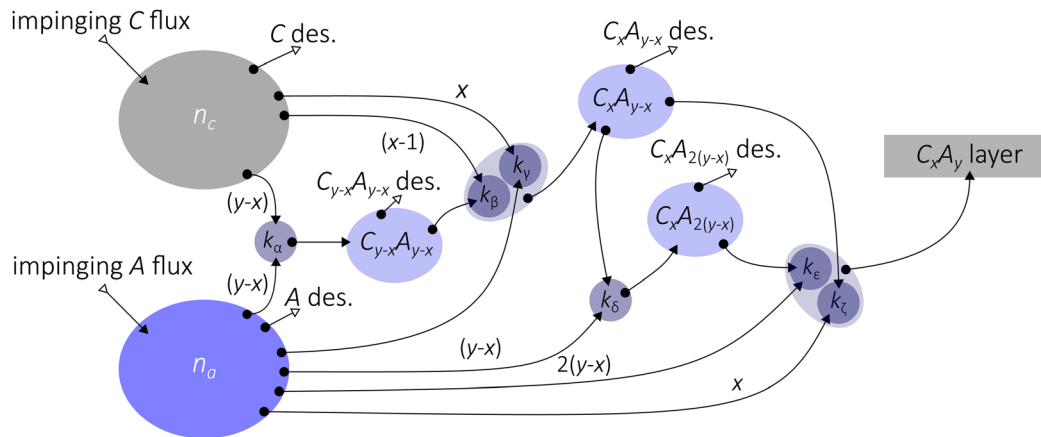
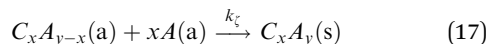
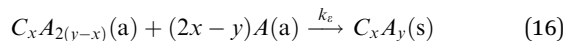
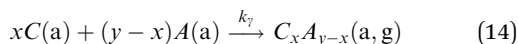
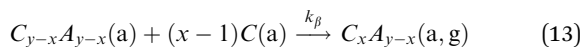
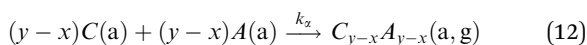


Fig. 5 MBE reaction scheme for binary III–VI and IV–VI materials, showing impinging  $\phi_c$  and  $\phi_a$ , resulting cation  $n_c$ , anion  $n_a$ , respective subcompound reservoirs, and the final compound  $C_xA_y$ . Chemical reactions (12)–(17) are indicated by reaction rate constants  $k_i$ .

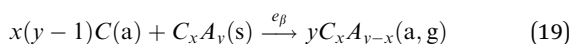
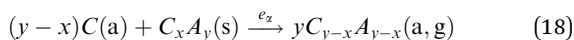
scheme depicted in Fig. 5 is an extension and refinement of the reaction scheme introduced in ref. 31.

Consecutive reaction pathways to form III–O, III–Se, IV–O, and IV–Se are:



with reaction rate constant  $k_i$  with  $i = \alpha, \beta, \gamma, \delta, \epsilon, \zeta$ . In eqn (13), the relation  $y - 1 = x$  is used. Note, for the growth of IV–VI compounds, reactions (13) and (16) are forbidden and reactions (15) and (17) are identical due to their stoichiometric coefficients  $x = 1$  and  $y = 2$ . Consequently, the surface reaction pathways for IV–VI are not as complex as for III–VI compounds.

It has been shown for III–O materials (e.g.,  $Ga_2O_3$ ) and IV–O materials (e.g.,  $SnO_2$ ) that these compounds can be chemically decomposed (etched) by their respective elemental metal (e.g., Ga or Sn) to form its respective suboxide (e.g., GaO,  $Ga_2O$ , or  $SnO$ )<sup>16</sup> via the reactions



with etching rate constants  $e_x$  and  $e_\beta$  to form the subcompounds  $C_{y-x}A_{y-x}$  (e.g., GaO or GaSe) and  $C_xA_{y-x}$  (e.g.,  $Ga_2O$  or  $Ga_2Se$ ), respectively. Note, for III–O materials only reaction (19) has been experimentally observed under MBE conditions.<sup>16</sup>

Finally, Fig. 6 plots our calculated  $\Delta G$  using eqn (20)–(24) as a function of  $T_G$  of  $Ga_2O_3$ ,  $Ga_2Se_3$ ,  $In_2O_3$ ,  $In_2Se_3$ ,  $SnO_2$ , and  $SnSe_2$  (calculations are given in the Appendix I). We calculated  $\Delta G$  for

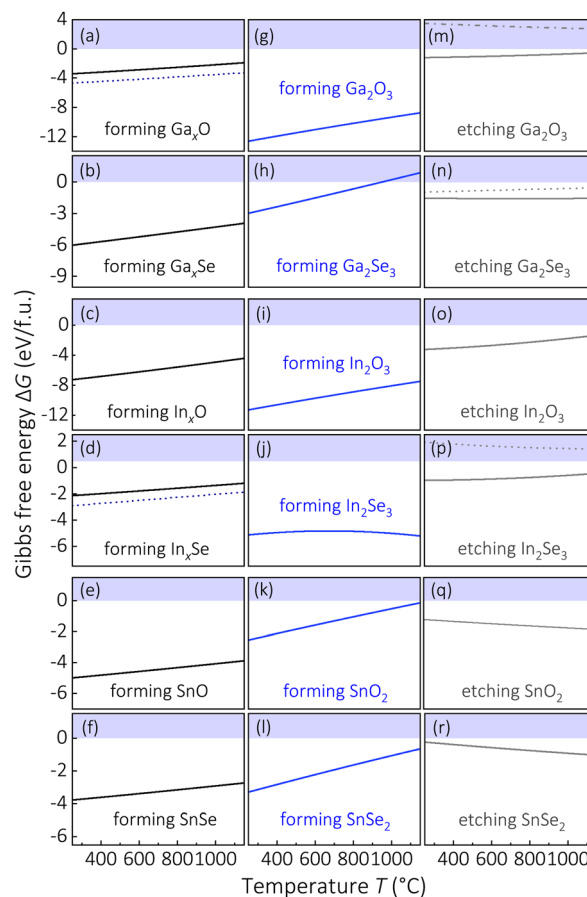


Fig. 6 The Gibbs energy ( $\Delta G$ ) as a function of temperature  $T$ . Values of  $\Delta G$  are in eV per formula unit (f.u.). (a)–(f)  $\Delta G$  for subcompound formations via eqn (12) [black solid lines] and eqn (13) [dark-blue dotted lines]. (g)–(l)  $\Delta G$  for solid thin film formations via eqn (17) [blue solid lines]. (m)–(r)  $\Delta G$  for thin film etching to form subcompounds via eqn (18) [gray dotted lines] and eqn (19) [gray solid lines].



growth and etch reactions (12)–(19) once data were available.<sup>52</sup> For all investigated materials and relevant  $T_G$ , the formation of the suboxide and subselenide is thermodynamically feasible. This is in agreement with the observed III-O and IV-O kinetics and we further calculate that III-Se and IV-Se compounds can be chemically decomposed by their elemental metal to form their respective subselenide through reactions (18) and (19). We thus conjecture that the formation of suboxides and subselenides is kinetically and thermodynamically favorable and the rate-limiting step for a wide-range of III-O, III-Se, IV-O, and IV-Se compound materials.

## V. Conclusions

We identify by published growth rate ( $\Gamma$ ) data of the  $\text{Ga}_2\text{O}_3$ ,  $\text{In}_2\text{O}_3$ , and  $\text{SnO}_2$  growth systems that the elements Ga, In, and Sn possess a higher reaction efficiency ( $\eta_M$ ) with adsorbed O than their corresponding volatile suboxides ( $\eta_S$ )  $\text{Ga}_2\text{O}$ ,  $\text{In}_2\text{O}$ , and  $\text{SnO}$ . We find that  $\eta_M \geq \eta_S$  and quantified the fundamental growth domain of III-VI materials whose regimes strongly depend on MBE growth conditions and find that  $\text{SFW} \geq \text{FGW}$ . In particular, we observe a vanishing M-rich growth regime with increasing  $T_G$ , leading to off-stoichiometric growth surfaces concerning their initially adsorbed densities of group III and group VI elements.

By combining a 2-step kinetic model to experimental  $\Gamma$  data of  $\text{Ga}_2\text{Se}_3$  with our thermodynamic analysis and calculations we find the volatile species for the  $\text{Ga}_2\text{Se}_3$ ,  $\text{In}_2\text{Se}_3$ , and  $\text{SnSe}_2$  systems are the subselenides  $\text{Ga}_2\text{Se}$ ,  $\text{In}_2\text{Se}$ , and  $\text{SnSe}$ , respectively. We provide a detailed reaction diagram for the growth of III-O, III-Se, IV-O, and IV-Se materials systems, supported by thermodynamic calculations.

The identified thermodynamic and kinetic feasibility of the proposed 2-step reaction mechanisms for III-Se and IV-Se materials let us conclude that III-Se and IV-Se compounds grow *via* (qualitatively) the same 2-step reaction mechanism—similar to what is established for III-O and IV-O materials.<sup>21,31,38</sup> To unambiguously identify the growth-rate-limiting steps and volatile species of the proposed binary III-O, III-Se, IV-O, and IV-Se growth systems [e.g., eqn (12)–(19)], *in situ* line-of-sight mass spectroscopy will reveal which subcompound is formed on the respective growth surface.

## Author contributions

Patrick Vogt: conceptualization (lead), data curation (lead), formal analysis (lead), investigation (lead), methodology (lead), writing original draft (lead). Shun-Li Shang: methodology (equal), data curation (equal), formal analysis (supporting), investigation (supporting), writing original draft (supporting). Zi-Kui Liu: data curation (supporting), investigation (supporting), methodology (supporting), writing original draft (supporting).

## Data availability

Data is available upon reasonable request from the corresponding authors.

## Conflicts of interest

The authors have no conflicts of interest to declare.

## Appendices

### Appendix I

Thin film growth *via* MBE takes place under isobaric-isothermal conditions. The change in the Gibbs energy  $\Delta G(T)$  at given temperature  $T$  is

$$\Delta G(T) = \Delta H(T) - T\Delta S(T), \quad (20)$$

with the change in enthalpy  $\Delta H(T)$  and the change in entropy  $\Delta S(T)$  determined as

$$\Delta H(T) = \Delta H_0 + \int_{T_0}^{T_G} dT C(T) \quad (21)$$

$$\Delta S(T) = \Delta S_0 + \int_{T_0}^{T_G} dT \left( \frac{C(T)}{T} \right), \quad (22)$$

respectively.  $\Delta H_0$  and  $\Delta S_0$  denote the change in  $\Delta H$  and  $\Delta S$  at room temperature,  $T_0 = 295$  K. The heat capacity  $C(T)$  is calculated as

$$C(T) = a + b 10^{-3}T + c 10^6 T^{-2} + d 10^{-6} T^2. \quad (23)$$

For all discussed species,  $\Delta H_0$ ,  $\Delta S_0$ ,  $a$ ,  $b$ ,  $c$ , and  $d$  are taken from ref. 52. A chemical reaction may occur spontaneously once  $\Delta G < 0$ . For a given reaction, with reactants  $R_i$  and products  $P_j$ , it can be determined by the sum of the Gibbs energies of  $P_j$ ,  $\sum_j G_{P_j}$ , minus the sum of the Gibbs energies of  $R_i$ ,  $\sum_i G_{R_i}$ , *i.e.*

$$\Delta G = \sum_j p_j G_{P_j} - \sum_i r_i G_{R_i}. \quad (24)$$

The stoichiometric coefficients of  $R_i$  and  $P_j$  are denoted as  $r_i$  and  $p_j$ , respectively.

## Acknowledgements

PV acknowledges the Max Planck Institute for Solid State Research for financial support and Martin Eickhoff and Alexander Karg for fruitful discussions regarding the reaction chemistries of III-O compounds. SLS and ZKL acknowledge the support from Endowed Dorothy Pate Enright Professorship at the Pennsylvania State University.

## References

- 1 J. R. Arthur, *J. Appl. Phys.*, 1968, **39**, 4032, DOI: [10.1063/1.1656901](https://doi.org/10.1063/1.1656901).
- 2 M. Copel, M. C. Reuter, E. Kaxiras and R. M. Tromp, *Phys. Rev. Lett.*, 1989, **63**, 632, DOI: [10.1103/PhysRevLett.63.632](https://doi.org/10.1103/PhysRevLett.63.632).
- 3 K. Ploog, *Annu. Rev. Mater. Sci.*, 1982, **12**, 123, DOI: [10.1146/annurev.ms.12.080182.001011](https://doi.org/10.1146/annurev.ms.12.080182.001011).



- 4 J. Neugebauer, T. K. Zywiets, M. Scheffler, J. E. Northrup, H. Chen and R. M. Feenstra, *Phys. Rev. Lett.*, 2003, **90**, 056101, DOI: [10.1103/PhysRevLett.90.056101](https://doi.org/10.1103/PhysRevLett.90.056101).
- 5 K. Ploog, *Annu. Rev. Mater. Sci.*, 1981, **11**, 171, DOI: [10.1146/annurev.ms.11.080181.001131](https://doi.org/10.1146/annurev.ms.11.080181.001131).
- 6 H. Riechert, R. Averbeck, A. Graber, M. Schienle, U. Straub and H. Tews, *MRS Online Proc. Libr.*, 1996, **449**, 149–159, DOI: [10.1557/PROC-449-149](https://doi.org/10.1557/PROC-449-149).
- 7 E. Calleja, M. A. Sánchez-García, F. J. Sánchez, F. Calle, F. B. Naranjo and E. Muñoz, *et al.*, *J. Cryst. Growth*, 1999, **201**, 296, DOI: [10.1016/S0022-0248\(98\)01346-3](https://doi.org/10.1016/S0022-0248(98)01346-3).
- 8 S. Fernández-Garrido, G. Koblmüller, E. Calleja and J. S. Speck, *J. Appl. Phys.*, 2008, **104**, 1, DOI: [10.1063/1.2968442](https://doi.org/10.1063/1.2968442).
- 9 Z. Zhu, M. Hagino, K. Uesugi, S. Kamiyama, M. Fujimoto and T. Yao, *Jpn. J. Appl. Phys.*, 1989, **28**, 1659, DOI: [10.1143/JJAP.28.1659](https://doi.org/10.1143/JJAP.28.1659).
- 10 K. Kato, M. Sano, K. Miyamoto and T. Yao, *Jpn. J. Appl. Phys.*, 2003, **42**, 2241, DOI: [10.1143/JJAP.42.2241](https://doi.org/10.1143/JJAP.42.2241).
- 11 L. Pfeiffer, K. W. West, H. L. Stormer and K. W. Baldwin, *Appl. Phys. Lett.*, 1989, **55**, 1888, DOI: [10.1063/1.102162](https://doi.org/10.1063/1.102162).
- 12 D. G. Schlom and L. N. Pfeiffer, *Nat. Mater.*, 2010, **9**, 881, DOI: [10.1038/nmat2888](https://doi.org/10.1038/nmat2888).
- 13 D. C. Tsui, H. L. Stormer and A. C. Gossard, *Phys. Rev. Lett.*, 1982, **48**, 1559, DOI: [10.1103/PhysRevLett.48.1559](https://doi.org/10.1103/PhysRevLett.48.1559).
- 14 M. E. White, M. Y. Tsai, F. Wu and J. S. Speck, *J. Vac. Sci. Technol., A*, 2008, **26**, 1300, DOI: [10.1116/1.2966423](https://doi.org/10.1116/1.2966423).
- 15 M. Y. Tsai, O. Bierwagen, M. E. White and J. S. Speck, *J. Vac. Sci. Technol., A*, 2010, **28**, 354, DOI: [10.1116/1.3294715](https://doi.org/10.1116/1.3294715).
- 16 P. Vogt and O. Bierwagen, *Appl. Phys. Lett.*, 2015, **106**, 081910, DOI: [10.1063/1.4913447](https://doi.org/10.1063/1.4913447).
- 17 P. Vogt, A. Mauze, F. Wu, B. Bonef and J. S. Speck, *Appl. Phys. Express*, 2018, **11**, 115503, DOI: [10.7567/APEX.11.115503](https://doi.org/10.7567/APEX.11.115503).
- 18 P. Vogt, F. V. E. Hensling, K. Azizie, J. P. McCandless, J. Park and K. DeLello, *et al.*, *Phys. Rev. Appl.*, 2022, **17**, 034021, DOI: [10.1103/PhysRevApplied.17.034021](https://doi.org/10.1103/PhysRevApplied.17.034021).
- 19 S. Raghuvansy, J. P. McCandless, M. Schowalter, A. Karg, M. Alonso-Orts and M. S. Williams, *et al.*, *APL Mater.*, 2023, **11**, 111113, DOI: [10.1063/5.0174373](https://doi.org/10.1063/5.0174373).
- 20 P. Vogt, F. V. E. Hensling, K. Azizie, C. S. Chang, D. Turner and J. Park, *et al.*, *APL Mater.*, 2021, **9**, 031101, DOI: [10.1063/5.0035469](https://doi.org/10.1063/5.0035469).
- 21 P. Vogt, D. G. Schlom, F. V. E. Hensling, K. Azizie, Z. K. Liu and B. J. Bocklund, *et al.*, *United States Patent*, 2022, 11462402, <https://patents.google.com/patent/US11462402B2/en>.
- 22 N. Teraguchi, F. Kato, M. Konagai, K. Takahashi, Y. Nakamura and N. Otsuka, *Appl. Phys. Lett.*, 1991, **59**, 567, DOI: [10.1063/1.105388](https://doi.org/10.1063/1.105388).
- 23 T. Okamoto, A. Yamada and M. Konagai, *J. Cryst. Growth*, 1997, **175**, 1045, DOI: [10.1016/S0022-0248\(96\)00984-0](https://doi.org/10.1016/S0022-0248(96)00984-0).
- 24 T. Shimada, F. S. Ohuchi, A. Koma and J. Jpn, *Appl. Phys.*, 1993, **32**, 1182, DOI: [10.1143/JJAP.32.1182](https://doi.org/10.1143/JJAP.32.1182).
- 25 G. Han, Z. G. Chen, J. Drennan and J. Zou, *Small*, 2014, **10**, 2747, DOI: [10.1002/sml.201400104](https://doi.org/10.1002/sml.201400104).
- 26 N. Balakrishnan, E. D. Steer, E. F. Smith, Z. R. Kudrynskiy, Z. D. Kovalyuk and L. Eaves, *et al.*, *2D Mater.*, 2018, **5**, 035026, DOI: [10.1088/2053-1583/aac479](https://doi.org/10.1088/2053-1583/aac479).
- 27 J. B. Varley, J. R. Weber, A. Janotti and C. G. Van de Walle, *Appl. Phys. Lett.*, 2010, **97**, 142106, DOI: [10.1063/1.3499306](https://doi.org/10.1063/1.3499306).
- 28 J. B. Varley, H. Peelaers, A. Janotti and C. G. Van de Walle, *J. Phys.: Condens. Matter*, 2011, **23**, 334212, DOI: [10.1088/0953-8984/23/33/334212](https://doi.org/10.1088/0953-8984/23/33/334212).
- 29 D. S. Liu, M. Hilse, A. R. Lupini, J. M. Redwing and R. Engel-Herbert, *ACS Appl. Nano Mater.*, 2023, **6**, 15029, DOI: [10.1021/acsanm.3c02602](https://doi.org/10.1021/acsanm.3c02602).
- 30 P. Vogt and O. Bierwagen, *Appl. Phys. Lett.*, 2016, **108**, 072101, DOI: [10.1063/1.4942002](https://doi.org/10.1063/1.4942002).
- 31 E. Ahmadi, O. S. Koksaldi, S. W. Kaun, O. Yuichi, D. B. Short and U. K. Mishra, *et al.*, *Appl. Phys. Express*, 2017, **10**, 041102, DOI: [10.7567/APEX.10.041102](https://doi.org/10.7567/APEX.10.041102).
- 32 Y. Oshima, E. Ahmadi, S. Kaun, F. Wu and J. S. Speck, *Semicond. Sci. Technol.*, 2018, **33**, 015013.
- 33 P. Vogt and O. Bierwagen, *Phys. Rev. Mater.*, 2018, **2**, 120401(R), DOI: [10.1103/PhysRevMaterials.2.120401](https://doi.org/10.1103/PhysRevMaterials.2.120401).
- 34 C. J. Frosch and C. D. Thurmond, *J. Phys. Chem.*, 1962, **66**, 877, DOI: [10.1021/j100811a027](https://doi.org/10.1021/j100811a027).
- 35 J. Valderrama-N and K. T. Jacob, *Thermochim. Acta*, 1977, **21**, 215, DOI: [10.1016/0040-6031\(77\)85019-3](https://doi.org/10.1016/0040-6031(77)85019-3).
- 36 R. Colin, J. Drowart and G. Verhaegen, *Trans. Faraday Soc.*, 1965, **61**, 1364, DOI: [10.1039/TF9656101364](https://doi.org/10.1039/TF9656101364).
- 37 P. Vogt, O. Brandt, H. Riechert, J. Lähnemann and O. Bierwagen, *Phys. Rev. Lett.*, 2017, **119**, 196001, DOI: [10.1103/PhysRevLett.119.196001](https://doi.org/10.1103/PhysRevLett.119.196001).
- 38 K. M. Adkison, S. L. Shang, B. J. Bocklund, D. Klimm, D. G. Schlom and Z. K. Liu, *APL Mater.*, 2020, **8**, 081110.
- 39 P. Vogt, *Growth Kinetics, Thermodynamics, and Phase Formation of group-III and IV oxides during Molecular Beam Epitaxy*, Humboldt University of Berlin, 2017, DOI: [10.18452/18036](https://doi.org/10.18452/18036).
- 40 L. N. Majer, T. Acartürk, P. A. Aken, W. Braun, L. Camuti and J. Eckl-Haese, *et al.*, *APL Mater.*, 2024, **12**, 091112, DOI: [10.1063/5.0224092](https://doi.org/10.1063/5.0224092).
- 41 S. Chae, H. Paik, N. M. Vu, E. Kioupakis and J. T. Heron, *Appl. Phys. Lett.*, 2020, **117**, 072105, DOI: [10.1063/5.0018031](https://doi.org/10.1063/5.0018031).
- 42 W. Chen, K. Egbo, H. Tornatzky, M. Ramsteiner, M. R. Wagner and O. Bierwagen, *APL Mater.*, 2023, **11**, 071110, DOI: [10.1063/5.0155869](https://doi.org/10.1063/5.0155869).
- 43 M. E. Davis and R. J. Davis, *Fundamentals of Chemical Reaction Engineering*, McGraw-Hill, 1221 Avenue of the Americas, New York, NY, 2003, 10020.
- 44 K. Sasak, A. Kuramata, T. Masui, E. G. Villora, K. Shimamura and S. Yamakoshi, *Appl. Phys. Express*, 2012, **5**, 035502.
- 45 K. Azizie, F. V. E. Hensling, C. A. Gorsak, Y. Kim, N. A. Pieczulewski and D. M. Dryden, *et al.*, *APL Mater.*, 2023, **11**, 041102, DOI: [10.1063/5.0139622](https://doi.org/10.1063/5.0139622).
- 46 A. Mauze, Y. Zhang, T. Itoh, F. Wu and J. S. Speck, *APL Mater.*, 2020, **8**, 021104, DOI: [10.1063/1.5135930](https://doi.org/10.1063/1.5135930).
- 47 F. Liu, T. K. Truttmann, D. Lee, B. E. Matthews, I. Laraib and A. Janotti, *et al.*, *Commun. Mater.*, 2022, **3**, 69, DOI: [10.1038/s43246-022-00290-y](https://doi.org/10.1038/s43246-022-00290-y).
- 48 Z. Wen, K. Khan, X. Zhai and E. Ahmadi, *Appl. Phys. Lett.*, 2023, **122**, 082101, DOI: [10.1063/5.0142107](https://doi.org/10.1063/5.0142107).



- 49 C. H. Ho, *ACS Omega*, 2020, 5, 18527, DOI: [10.1021/acsomega.0c02623](https://doi.org/10.1021/acsomega.0c02623).
- 50 Scientific Group Thermodata Europe (SGTE) Thermodynamic Properties of Inorganic Materials, in *Lehrstuhl fuer Theoretische Huettenkunde* (Ed), Landolt-Boernstein New Ser Gr IV, Springer, Verlag Berlin Heidelberg, 1999, vol. 19A.
- 51 J. O. Andersson, T. Helander, L. Hoglund, P. Shi and B. Sundman, Thermo-Calc DICTRA: computational tools for materials science, *Calphad*, 2002, 26, 273.
- 52 M. Binnewies and E. Mielke, *Thermochemical Data of Elements and Compounds*, Wiley VCH, 2nd edn, 2002, DOI: [10.1002/9783527619818](https://doi.org/10.1002/9783527619818).

